RECENT ADVANCES IN

Breast Imaging, Mammography, and Computer-Aided Diagnosis of Breast Cancer

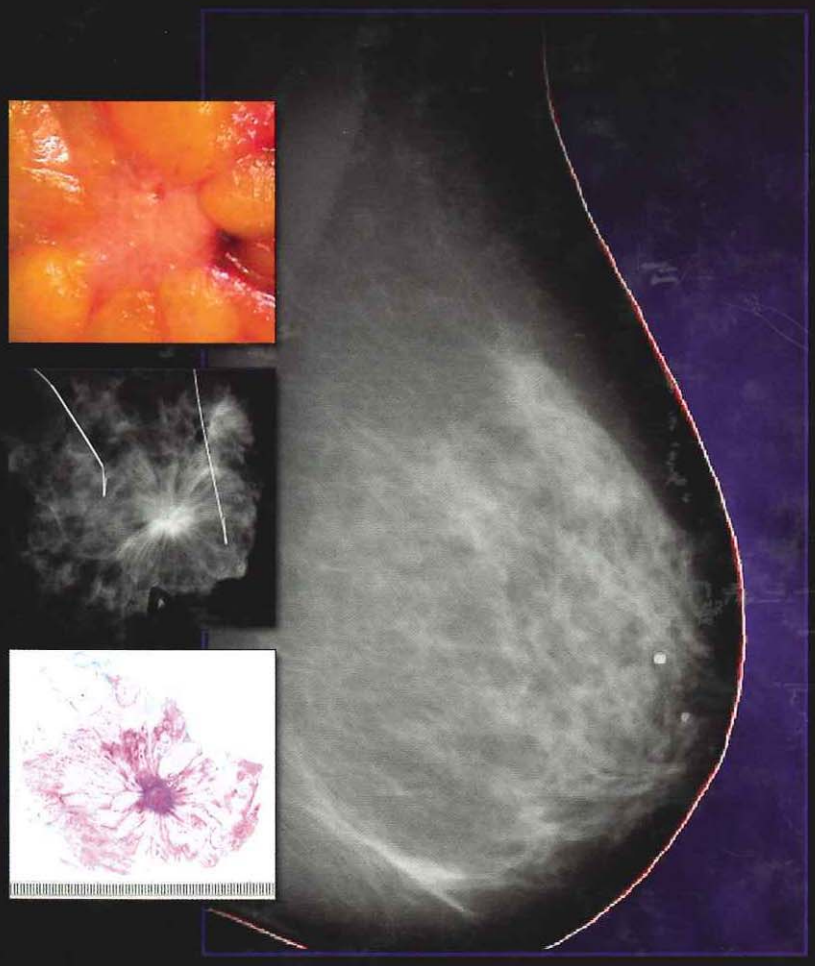

Jasjit S. Suri

Rangaraj M. Rangayyan

Editors

RECENT ADVANCES IN

Breast Imaging, Mammography, and Computer-Aided Diagnosis of Breast Cancer

Jasjit S. Suri
Rangaraj M. Rangayyan
Editors

Breast cancer is the most common type of cancer in women worldwide. About ten percent of women are confronted with breast cancer in their lives. Breast cancer can be most efficiently treated if detected at an early stage. This book focuses on the application of computer vision for lesion identification in mammograms and breast imaging volumes called computer-aided diagnosis (CAD). The book is divided into four parts: Part I presents the anatomic, histopathology, and mammographic views of the breasts, and the physics of different breast imaging modalities. Part II presents the techniques for lesion and mass detection through CAD. Part III presents the applications of different computer vision fields in breast-image registration. Finally, Part IV presents the performance evaluation section for breast CAD techniques.

Jasjit S. Suri, Ph.D. is an innovator, scientist, a visionary, an industrialist and an internationally known world leader in Biomedical Engineering/Sciences. Dr. Suri has spent over 20 years in the field of biomedical engineering of devices and its management. He received his Doctorate from the University of Washington, Seattle, and Master's in Executive Business Management from Weatherhead, Case Western Reserve University, Cleveland, Ohio. Dr. Suri was presented with the President's Gold Medal in 1980, and was recently elected as a Fellow of the American Institute for Medical and Biological Engineering.

Rangaraj M. Rangayyan, Ph.D. holds the distinguished "University Professorship" in Biomedical Signal and Image Analysis at the University of Calgary, Alberta, Canada, where he also served as an Associate Vice-President of Research. He is a pioneer in the field of computer-aided diagnosis and is a Fellow of the IEEE, AIMBE, SPIE, and EIC. Rangayyan's research interests are in the areas of digital signal and image processing, biomedical signal and image analysis, medical imaging and computer vision.

ISBN 081946081-8
90000
9 790819 460812

SPIE Press
P.O. Box 10
Bellingham, WA 98227-0010

ISBN: 0-8194-6081-8
SPIE Vol. No.: PM155

The International Society for Optical Engineering

CHAPTER 16

DETECTION, CHARACTERIZATION, AND VISUALIZATION OF BREAST CANCER USING 3D ULTRASOUND IMAGES

Daisuke Fukuoka
Takeshi Hara
Hiroshi Fujita
Gifu University, Japan

CONTENTS

16.1 INTRODUCTION

Breast cancer is one of the most common diseases for women. Early detection of breast cancer may decrease the cost of treatments and improve the quality of life of the patients. While screening mammography plays an important role in detecting cancers at an early stage, ultrasonography is employed as a noninvasive diagnostic examination.

Breast cancer screening using mammography has been introduced in Japan for over-50-year-old women by governmental recommendation. Examinations with ultrasound images also being discussed for over-40-year-old women whose breasts tend to be dense, because small nonpalpable masses hidden by normal structures, such as mammary glands, may be shown on ultrasound images.

In Japan, mammographic breast cancer screening for women aged over 50 was introduced in 2003 with governmental recommendation. In addition, examination using ultrasound images for women over 40 has been discussed. This is because younger breasts tend to be denser. Small nonpalpable masses can be hidden by normal structures such as mammary glands that are occult on mammograms. Ultrasound imaging may be used to depict these masses. Some regions in Japan have already employed the screening programs with ultrasounds before the governmental recommendation of mammographic examination. Whole breast scanning devices with Octson mechanisms have been used for diagnosis in three decades.

Screening with mammography computer-aided diagnosis (CAD) and ultrasound has been carried out at private hospitals in Japan. Ultrasound images are employed to determine whether the mass findings using CAD systems are true or false shadows.

Although many researchers have reported their work on mammogram CAD systems, there are very few studies concerning breast ultrasound CAD systems K. Drukker, K. Horsch and Giger et al.[1–5] is have reported fundamental approachs to detect and to classify lesions in breasts. CAD schemes for breast masses using free-hand probes and 3D imaging devices have been developed.[6,7] The scheme consists of three steps: detection, classification, and visualization of masses. The detection of masses is based on active-contour and balloon models in 2D and 3D spaces. The visualization technique provides virtual B- and C-mode images to confirm the shape and the position of the lesion in the breast. Details of the detection, classification, and visualization techniques are described in the following sections.

16.2 MATERIAL AND METHODS

In the examination using ultrasound devices, the image acquisition and the diagnostic procedure share the examination time. This is the essential difference in the work flow of CAD ultrasound devices and other types of CAD. In the lung CAD

scheme using multirow CT units, for example, there are time differences for the data acquisition before the interpretation. Most of the diagnosis using ultrasound devices is made while the examination is performed.

Some parts of the CAD system must have the real-time response for diagnosis since the delay of the scanning or the lack of the frame including lesions lead to loss of the patient merits.

Figure 16.1 shows the overview of our CAD scheme using the ultrasound devices. Data acquisitions from breasts are performed using a hand probe or 3D probe. The digital image data in DICOM format is separated in 2D data because the volume data of the breast is stored in many 2D-plane images. The NTSC outputs (video signal) from the ultrasound device is also employed to capture the 2D data if the DICOM outputs are not available.

The volume data is reconstructed from the many 2D images interpolating the voxel values to be the data in the isotropic scale. The interpolation using the hypercubic method was employed if the original data was not isotropic. The detection, classification, and visualization of the data are performed by employing the isotropic volume data.

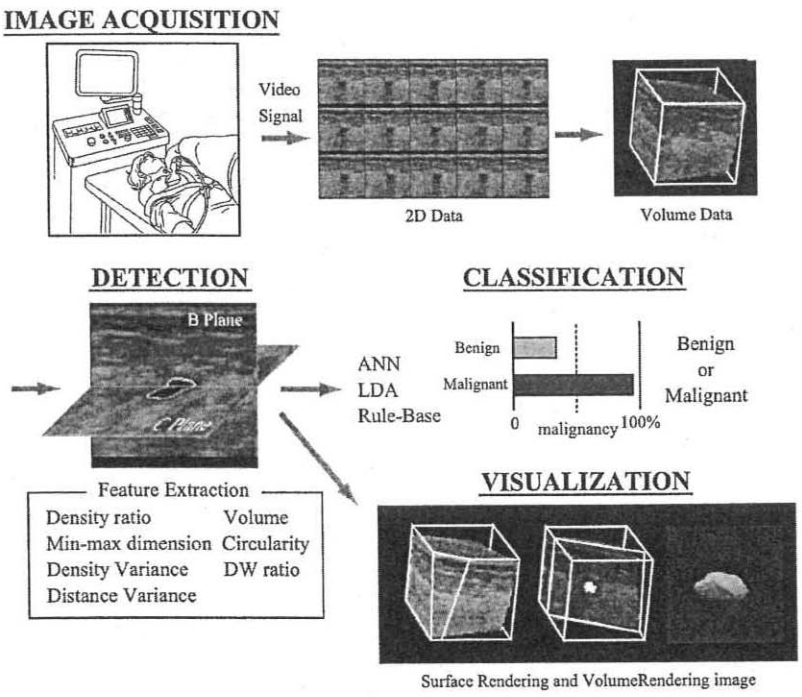

Figure 16.1 Overview of CAD workflow using 3D untrasound devices. After image acquisition from patients, image interporation is performed to create the isotropic data. Detection, classification, and visualization are performed using the isotropic data.

16.2.1 DATABASE

The 3D images employed in this study were obtained using the equipment by Medison Co.* A single probe with scanning dimensions of 5 cm × 5 cm was used. This Medison device was mainly applied to classify the breast masses previously detected by other modalities, such as mammography or palpations, because of the narrow area of the scanning. The pixel size of the images was within 256 × 256 × 256, and the scan was examined in a few seconds while the probe was moved mechanically.

16.2.2 DETECTION AND SEGMENTATION

The segmentation of a mass region on an ultrasound image is generally difficult because the signal is week and noisy. Moreover, the posterior echo is eliminated by the nature of solid masses. Lesion segmentation is often an important step in CAD schemes. Some techniques were used to approximate the boundary in order to extract the feature values from the shape and/or the area of masses. Segmentation methods based on energy minimization models have been explored by various researchers.[7–12]

16.2.2.1 3D active balloon model

The active balloon model (ABM),[13] a kind of active contour model in 3D spaces were applied, to determine the boundaries around masses. The continuity of the ABM contour is controlled by internal and external forces. The energy function of the ABM contour, $E_{\text{contour}}(x)$, is defined as

$$E_{\text{contour}}(x) = E_{\text{int}}(x) + E_{\text{ext}}(x), \tag{16.1}$$

where the internal and the external energy functions $E_{\text{int}}(x)$ and $E_{\text{ext}}(x)$ are defined as

$$E_{\text{int}}(x) = \alpha \sum_{i=0}^{5} \left\{ \max_{j \in \{x, \text{connected to another points}\}} [\mathbf{p}(i) - \mathbf{p}(x)] \cdot \mathbf{e}_i \right\}^2, \tag{16.2}$$

and

$$E_{\text{ext}}(x) = k \sum_{i \in \{\text{sample points}\}} -G_\sigma \{[\mathbf{p}(i) - \mathbf{p}(x)]\} \tag{16.3}$$

where $\mathbf{p}(x)$ represents the 3D vector at point x, and $\mathbf{e}_i$ is the unit vector at point x, such as $\mathbf{e}_0(1, 0, 0)$, $\mathbf{e}_1(-1, 0, 0)$, $\mathbf{e}_2(0, 1, 0)$, $\mathbf{e}_3(0, -1, 0)$, $\mathbf{e}_4(0, 0, 1)$, $\mathbf{e}_5(0, 0, -1)$.

*Seoul, Korea.

G_σ is a Gaussian function of standard deviation σ

$$G_\sigma(x) = \frac{1}{\sqrt{2\pi\sigma}} \exp \frac{-\mathbf{x} \cdot \mathbf{x}}{2\sigma^2}. \tag{16.4}$$

Figure 16.2 shows a simple example of ABM. The example illustrates that the initial balloon (left) of polyhedrons (1280 triangle polygons) that sit inside a cube, and the balloon extends to fill the cube (right). All vertices were controlled based on the energy function outputs defined by the internal and external energies. The energies were calculated by the intensity and the directions among the normal vectors connecting the apex.

Figure 16.3 shows an example of a mass region extraction using the active balloon method. The white bold curves show the changes in the extracted contour (left to right). The direction of the gradient vector along the boundary was computed and energy minimization was iterated 100 times. The area of the mass was determined by the ACM. A feature extraction approach based on the shape and boundaries of the masses was applied to the determined area.

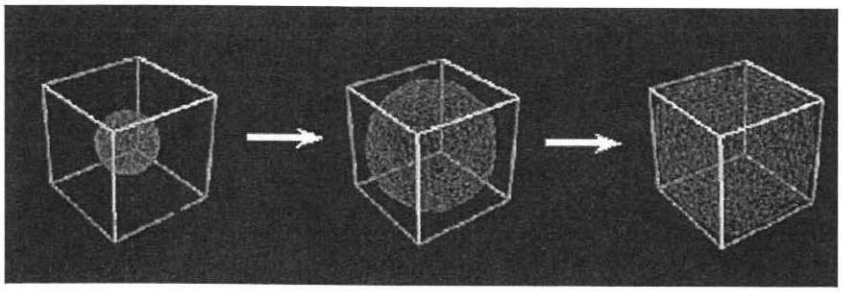

Figure 16.2 An example of balloon extension in a cube. The initial node (left) shows a sphere shape because the nodes were set on the sphere surface. The distances between the nodes increase, keeping the sphere shape (middle). The sphere shape does not change until the nodes touch the boundaries or the limitation of energy functions. Most of the nodes stop at the cube surface (right) because of the limitation of the energy function; however, some nodes around the cube corners indicate the original sphere surface.

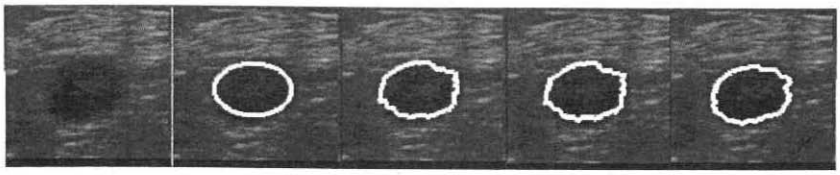

Figure 16.3 An example of shape changes in region extraction using the active balloon model. The left image shows the original signal with a obvious mass. The extracted shape changes from a simple circle to a complex boundary (left to right). Actually, the boundary has a 3D surface; however, the boundary slice at the maximum area of the mass was shown in this example.

16.2.3 CLASSIFICATION

Classifying masses using ultrasonograms may help in reducing the number of biopsies performed on benign lesions. For the classification of benign and malignant masses, several characteristic features such as shape, echogenic halo, internal echoes, and posterior echoes must be identified. Most of these features require the segmentation of mass lesions from the normal background. The detection and region-extraction techniques mentioned before play an important role in determining the boundaries of mass signals. Table 16.1 lists the physical characteristics related to benign and malignant lesions. The classification scheme employed the following eight features in classifying masses:

(1) Depth-to-width ratio in 3D, calculated by dividing the mass area (in number of pixels) on the x–z plane by the mass area on y–z plane.
(2) Ratio between the min-max dimensions, where each of the mass dimension was determined by measuring the maximum and minimum distance within the mass region.

    The distances between any two points on the boundary were calculated. The maximum and minimum distances were taken as the maximum and minimum dimensions of the mass, respectively.
(3) Volume of mass, defined by the regions indicated by the ABM.
(4) Density variance within the anterior region. A 20-pixels thick outershell was generated by expanding the final ABM in all directions using 3D-morphological processing. The outershell was then sectioned into three regions: the anterior region, the posterior region, and the lateral region. Figure 16.4 shows the cross section of a mass with the three regions demonstrated. Density variance was calculated with in the anterior region.
(5) Variance of density in the internal area, which has shown in the center region in Fig. 16.4. The variance of density was calculated.
(6) Variance of distance from center of gravity to boundary, calculated by measuring from the center of gravity to the nodes of the ABM.
(7) Circularity of the region, determined by the ratio of the volume and surface area.
(8) Density ratio of anterior and posterior region, determined the same as in feature (4). The density ratio of the anterior and posterior echo region was

Table 16.1 Lesion characteristics.

Sonographic features	Benign	Malignant
Lesion shape	Ellipsoid	Irregular
Border	Smooth	Rough
Internal echoes	Homogeneous	Heterogeneous
Posterior echoes	Enhanced	Attenuated
Edge shadows	Extreme	Absent

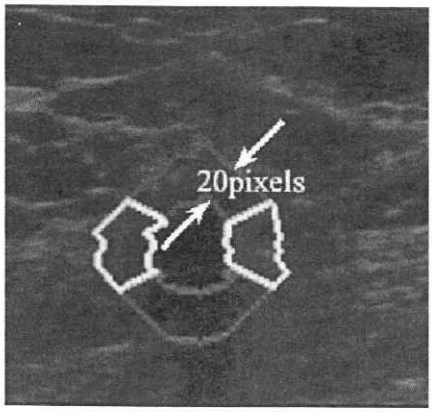

Figure 16.4 The surrounding of mass devided into three regions of upper (anteria), torus (lateral), and lower (posterior).

calculated. The intensity of the anterior echo tended to be attenuated when the mass was a malignant one, because a solid mass absorbed much of the sound signals and did not reflect to the probe.

Rule-based classification methods, referring to the discriminant plane from the linear discriminant analysis (LDA), drive out disparate feature values, and classify specific features as benign or malignant.

A three-layer artificial neural network (ANN) with eight input units, twelve hidden units, and an output unit was also employed as a nonlinear classifier. The ANN structure was determined experimentally and was trained based on a back-propagation algorithm. The training set consisted of typical malignant and benign cases with standardized features.

16.2.4 VISUALIZATION PROCESS

The display of the 3D images is very important for recognizing the mass shape and distribution of echo signals. Volume- and surface-rendering techniques were often employed to visualize the high-dimensional data for CT and MR images showing the 3D structures of organs and vessels. The rendering techniques can also be applied to the 3D ultrasound images using the intensity of the ultrasound signals instead of the CT values or the MR signals.

The mass regions are visualized by using volume-rendering and surface-rendering approaches. Figure 16.5 shows examples of a 3D display by using the volume-rendering technique. A series of three clippings (front to back) of the same plain of a mass region is shown. The scan images in any directions (planes) were shown by moving the mouse to indicate the angle of view. Figures 16.6 and 16.7 show examples of surface rendering results of benign and malignant masses, respectively. The rough surface of the malignant masses was well recognized in

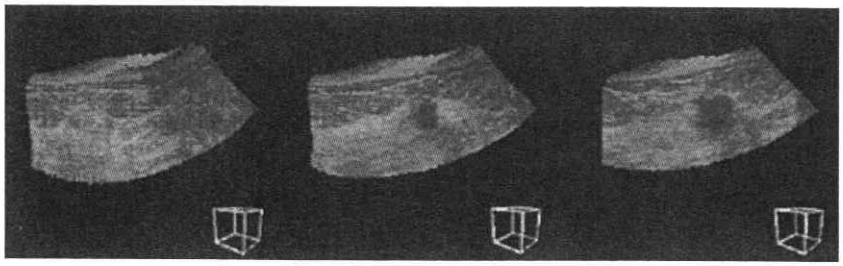

Figure 16.5 Examples of volume-rendering images. Three different clippings of a mass region are shown.

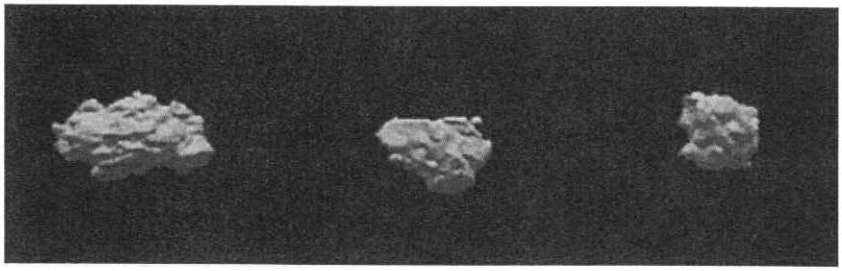

Figure 16.6 Examples of surface-rendering images. Three different malignant masses are shown.

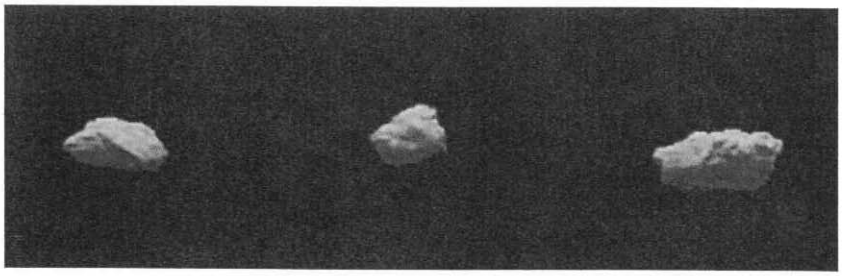

Figure 16.7 Examples of surface-rendering images. Three different benign masses are shown.

Fig. 16.6. The benign masses in Fig. 16.7 depict smoother surfaces. Emphasizing the shadows created by artificial lights in the space was very effective in visualizing the shape of the mass.

16.3 RESULTS

By employing 227 cases (147 benign, 80 malignant), the classification performance was found with a sensitivity of 76% (61/80) and a specificity of 71% (104/147). The cases tested were difficult to classify by well-experienced physicians using only ultrasound images, so this result may be adequate as an initial experiment.

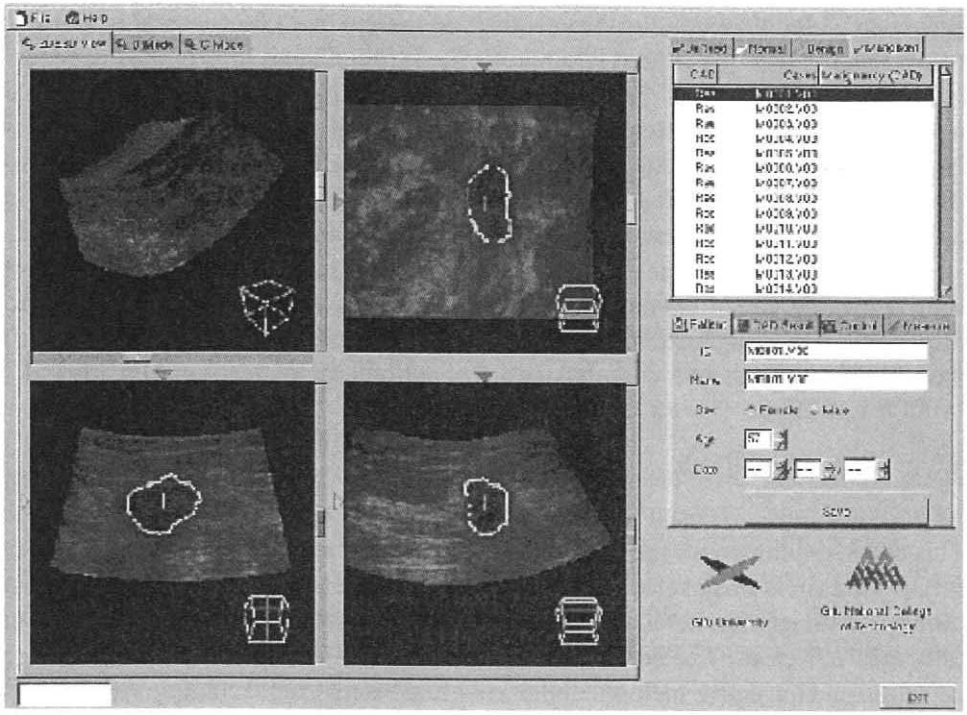

Figure 16.8 Overview of graphical user interface of our CAD system. Volume-rendering and two types of B-mode images are shown (upper left and lower two, respectively). C-mode image reconstructed from the volume data is on the upper right. The boundary of the mass extracted by the balloon model is also indicated. Refer to the CD for the full color figure.

Figure 16.8 shows the user interface of our CAD system. Volume-rendered images and the patient's lists are shown in the same window. The volume-rendered image can be rotated by moving the mouse to a desired angle of view, and the positions of clipping the planes were determined by the same the mouse movement. There are four windows for image display. Axial and sagital in the CT view are also a common view for the diagnosis in ultrasound images, because the images are reconstructed along the direction of the sonic from the probe (lower two images in 16.8). C-mode has a new comprehensive coronal view in CT diagnosis (upper right in 16.8).

16.4 DISCUSSIONS

Data acquisition, especially acquisition using NTSC signal, may have a great influence on the detection and classification performance. The technologist often varies the dynamic range and the gain for the various patients to make diagnosis easier.

Volume-data reconstruction from hand-probe image data may be impossible without registration devices such as the 3D tracking device developed by

Polhemus.[14] In this work, the data acquisition system has a mechanical movement below the breast of the patient lying prone on a specially equipped bed.

CAD parameters also have an influence on the performance. The artificial neural network has been tested using a leave-one-out method, however the rule-based methods have an experimental approach to exclude the outstanding candidates with extraordinary feature values. The rest of the candidates were entered in the linear discriminant analysis (LDA) to create the classification plane.

The 3D view of volume data may cost more time in an examination. To collect the 3D volume, the probe must move around the breast. The B-mode view is also displayed on the diagnostic monitor, but the 3D image could not be rendered until the whole breast area was captured, and acquisition time depends on the probe.

16.5 CONCLUSIONS

This chapter summarizes the detection, classification, and visualization techniques for 3D ultrasound images for breast cancer. A CAD system for masses on 3D breast ultrasound images has been developed based on the preliminary performance of an estimated 227 cases. The detection and classification methods were based on edge detection and the active balloon model. A volume-rendering technique was applied to prepare the 3D images. The initial results achieved a sensitivity of 76% and a specificity of 71%. It was concluded that this scheme would be effective for the diagnostic aid of ultrasound images for breast diseases.

REFERENCES

1. M.L. Giger, H. AI-Hallaq, Z. Huo, C. Moran, D.E. Wolverton, C.W. Chan, and W. Zhong, "Computerized analysis of lesions in US images of the breast." *Acad. Radiology* **6**(11), pp. 665–674 (1999).
2. K. Drukker and M.L. Giger, "Computerized analysis of shadowing on breast ultrasound for improved lesion detection." *Med. Phys.* **30**(7), pp. 1833–1842 (2003).
3. K. Drukker, M.L. Giger, K. Horsch, M.A. Kupinski, and C.J. Vyborny, "Computerized lesion detection on breast ultrasound." *Med. Phys.* **29**(7), pp. 1438–1446 (2002).
4. K. Drukker, M.L. Giger, C.J. Vyborny, and E.B. Mendelson, "Computerized detection and classification of cancer on breast ultrasound." *Acad. Radiology* **11**(5), pp. 526–535 (2004).
5. K. Horsch, M.L. Giger, C.J. Vyvorny, and L.A. Venta, "Performance of computer-aided diagnosis in the interpretation of lesions on breast sonography." *Acad. Radiology* **11**(3), pp. 272–280 (2004).
6. D. Fukuoka, T. Hara, H. Fujita, T. Endo, and Y. Kato, "Automated detection and classification of masses on breast ultrasonograms and its 3D imaging tech-

nique." *IWDM 2000: 5th International Workshop on Digital Mammography*, M.J. Yaffe (ed.), Medical Physics Publ., Madison, WI, pp. 182–188 (2001).
7. D. Fukuoka, T. Hara, H. Fujita, T. Endo, and Y. Kato, "Dynamic region-contour-extraction method with automated initial-contour production and unification of contours." *Trans. Inst. Electron., Info. Commun. Eng.* **J81-D-II**(6), pp. 1448–1451 (1998).
8. M. Kass, A. Witkin, and D. Terzopoulos, "Snakes: active contour models." *Int. J. Comput. Vision* **1**(1), pp. 321–331 (1988).
9. K. Horsch, M.L. Giger, L.A. Venta, and C.J. Vyborny, "Automatic segmentation of breast lesions on ultrasound." *Med. Phys.* **28**(8), pp. 1652–1659 (2001).
10. T. Hara, D. Fukuoka, H. Fujita, T. Endo, and W.K. Moon, "Development of automated detection and classification methods of masses on 3D breast ultrasound images." *CARS2002*, pp. 794–799 (2002).
11. R.-F. Chang, W.-J. Wu, C.-C. Tseng, D.-R. Chen, and W.K. Moon, "3D snake for US in margin evaluation for malignant breast tumor excision using mammotome." *IEEE Trans. Info. Technol. Biomed.* **7**(3), pp. 197–201 (2003).
12. B. Sahiner, H.-P. Chan, M.A. Roubidoux, M.A. Helvie, L.M. Hadjiiski, A. Ramachandran, C. Paramagul, G.L. LeCarpentier, A. Nees, and C. Blane, "Computerized characterization of breast masses on three-dimensional ultrasound volumes." *Med. Phys.* **31**(4), pp. 744–754 (2004).
13. K. Tsuchiya, H. Matsuo, and A. Iwata, "3D shape reconstruction from range data using active balloon model and symmetry restriction." *Trans. Inst. Electron., Info. Commun. Eng.* **J76-D-II**(9), pp. 1967–1976 (1993).
14. Polhemus Co. Webpages: http://www.polhemus.com.